

**PL-TR-96-2300**

# **SOURCE FUNCTIONS OF NUCLEAR EXPLOSIONS FROM SPECTRAL SYNTHESIS AND INVERSION**

**Peter Puster  
Thomas H. Jordan**

**Massachusetts Institute of Technology  
Department of Earth, Atmospheric, and Planetary Sciences  
Cambridge, MA 02139**

**20 November 1996**

**Scientific Report No. 1**

**APPROVED FOR PUBLIC RELEASE; DISTRIBUTION UNLIMITED**

**19970311 120**



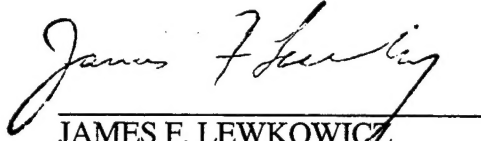
**PHILLIPS LABORATORY  
Directorate of Geophysics  
AIR FORCE MATERIEL COMMAND  
HANSCOM AFB, MA 01731-3010**

**DTIC QUALITY INSPECTED 3**

This technical report has been reviewed and is approved for publication.



DELAINE R. REITER  
Contract Manager  
Earth Sciences Division



JAMES F. LEWKOWICZ  
Director  
Earth Sciences Division

This report has been reviewed by the ESD Public Affairs Office (PA) and is releasable to the National Technical Information Service (NTIS).

Qualified requestors may obtain copies from the Defense Technical Information Center. All others should apply to the National Technical Information Service.

If your address has changed, or you wish to be removed from the mailing list, or if the addressee is no longer employed by your organization, please notify PL/IM, 29 Randolph Road, Hanscom AFB, MA 01731-3010. This will assist us in maintaining a current mailing list.

Do not return copies of this report unless contractual obligations or notices on a specific document requires that it be returned.

REPORT DOCUMENTATION PAGE			Form Approved OMB No. 0704-0188	
Public reporting burden for this collection of information is estimated to average 1 hour per response, including the time for reviewing instructions, searching existing data sources, gathering and maintaining the data needed, and completing and reviewing the collection of information. Send comments regarding this burden estimate or any other aspect of this collection of information, including suggestions for reducing this burden, to Washington Headquarters Services, Directorate for Information Operations and Reports, 1215 Jefferson Davis Highway, Suite 1204, Arlington, VA 22202-4302, and to the Office of Management and Budget, Paperwork Reduction Project (0704-0188), Washington, DC 20503.				
1. AGENCY USE ONLY (Leave Blank)	2. REPORT DATE <b>20-Nov-96</b>	3. REPORT TYPE AND DATES COVERED <b>Scientific Report 1</b>		
4. TITLE AND SUBTITLE <b>"Source Functions of Nuclear Explosions from Spectral Synthesis and Inversion"</b>		5. FUNDING NUMBERS <b>Contract # F19628-95-C-0102 PE 62101F TR 7600 TA GM WU AB</b>		
6. AUTHOR(S) <b>Peter Puster, Thomas H. Jordan</b>		8. PERFORMING ORGANIZATION REPORT NUMBER		
7. PERFORMING ORGANIZATION NAME(S) AND ADDRESS(ES) <b>Massachusetts Institute of Technology Department of Earth, Atmospheric, and Planetary Sciences Cambridge, MA 02139</b>		10. SPONSORING/MONITORING AGENCY REPORT NUMBER  <b>PL-TR-96-2300</b>		
9. SPONSORING/MONITORING AGENCY NAME(S) AND ADDRESS(ES) <b>Phillips Laboratory 29 Randolph Road Hanscom AFB, MA 01731-3010 Contract Manager: Delaine Reiter/GPE</b>		11. SUPPLEMENTARY NOTES		
12a. DISTRIBUTION/AVAILABILITY STATEMENT <b>Approved for public release; distribution unlimited.</b>		12b. DISTRIBUTION CODE		
13. ABSTRACT (Maximum 200 words)  We apply methods for the recovery of the frequency-dependent moment-rate tensor, $M(\omega)$ , to the study of Lop Nor nuclear explosions. This approach encompasses many source parameter diagnostics that have been traditionally used to discriminate nuclear explosions from chemical explosions and earthquakes and has the potential to provide new discrimination tools. We parameterize the source as $M(\omega) = M_I(\omega) + M_D(\omega)$ , where $M_I(\omega)$ and $M_D(\omega)$ are isotropic and deviatoric components, respectively. Our goal is to quantify both isotropic and deviatoric components, and investigate the different contributions to $M_D(\omega)$ , in particular the tectonic release. Since tectonic release can bias estimates of $M_I(\omega)$ and may limit discrimination capabilities of sparse networks, it is important to be able to characterize the amount of tectonic release – in particular as a function of frequency. Our approach uses synthetic seismograms to improve the localization of signal measurements in both time and frequency domains. We adapt our earthquake-source inversion algorithms to account for isotropic sources at very shallow depths. We test our algorithms using a synthetic case with a known moment-tensor source composed in equal parts of isotropic and deviatoric sources; we successfully recover both $M_D$ and $M$ using body waves and surface waves on horizontal and vertical components. We apply our methods to a data set containing both $SH$ and Love waves as well as the body-wave portion between $P$ and $R_1$ and the minor-arc Rayleigh waves from the 92/5/21 Chinese nuclear test. We recover a significant tectonic release component for this event; the deviatoric moment tensor is a dip-slip reverse fault with a scalar moment $M_D = 1.9 \pm 0.2 \times 10^{17}$ Nm. The strike of the best-fitting double-couple is $320^\circ$ . The source-time function derived from $SH$ -polarized waves shows some complexity, with a sharp pulse in moment release followed by a long, smooth tail. The former is hypothesized to be explosion energy scattered in $SH$ waves by near-source heterogeneities, and the latter appears to be an earthquake-like component of tectonic release. At low frequencies, the scalar moment ratio is $M_D/M_I = 0.61 \pm 0.01$ .				
14. SUBJECT TERMS <b>Lop Nor nuclear test, frequency-dependent moment-tensor, tectonic release, spectral inversion, source-time function</b>			15. NUMBER OF PAGES <b>32</b>	
17. SECURITY CLASSIFICATION OF REPORT <b>Unclassified</b>			16. PRICE CODE	
18. SECURITY CLASSIFICATION OF THIS PAGE <b>Unclassified</b>		19. SECURITY CLASSIFICATION OF ABSTRACT <b>Unclassified</b>		20. LIMITATION OF ABSTRACT <b>SAR</b>

# CONTENTS

<b>Objectives and Approach</b>	<b>1</b>
<b>Research Accomplishments</b>	<b>4</b>
<b>Modifications to the Analysis Procedures</b>	<b>4</b>
<b>Synthetic Test Case</b>	<b>5</b>
<b>Lop Nor Nuclear Test From May 21, 1992</b>	<b>10</b>
<b>Summary and Conclusions</b>	<b>18</b>
<b>References</b>	<b>20</b>



## Objectives and Approach

The seismological problem most relevant to nuclear monitoring under a Comprehensive Test Ban Treaty (CTBT) is to discriminate small nuclear explosions from chemical explosions and small earthquakes in a variety of geological settings. The dual challenges posed by the desire for a small detection threshold and a global reach, which includes areas of low seismicity, call for an approach to discriminate nuclear explosions from chemical explosions and earthquakes that simultaneously uses multiple diagnostics, such as  $M_s$ - $m_b$  ratio, radiation pattern, and amplitude spectrum. A general method for studying seismic sources that encompasses many traditional source parameter discriminants is based on the recovery of the broad-band moment-rate tensor,  $\mathbf{M}(\omega)$ . This moment tensor can be modeled as the product of a complex function,  $f(\omega)$ , whose inverse Fourier transform is the source-time function,  $f(t)$ , and a time-independent mechanism tensor,  $\hat{\mathbf{M}}$ , usually taken to be the (zeroth-order) spatial moment of the stress glut-rate tensor [Backus, 1977; Silver and Jordan, 1982]. In explosion seismology, the source-time function is often equated to the reduced displacement potential (RDP),  $\psi(t)$ , via  $f(t) = 4\pi\rho\alpha^2\dot{\psi}(t)$  [e.g., Denny and Johnson, 1991]. More generally, however, several processes contribute to  $\mathbf{M}(\omega)$ ; these include the release of tectonic prestress, spall and slapdown, as well as the RDP of the explosion itself.

The comprehensive nature of an approach based on recovering  $\mathbf{M}(\omega)$  is appealing. For example, writing  $f(\omega) = A(\omega)e^{i\Delta t(\omega)}$  in polar form illustrates that the amplitude spectrum,  $A(\omega)$ , is just the modulus of  $f(\omega)$ . Furthermore, to the extent that good synthetic seismograms can be computed from  $\mathbf{M}(\omega)$ , relative excitations of different waves (e.g.,  $M_s$ - $m_b$  ratio) can also be obtained. In addition, several new types of discriminants are potentially derivable from  $f(\omega)$ . The moment-tensor approach is amenable for setting up inverse problems to separate the isotropic explosion component,  $\mathbf{M}_I(\omega) = M_I(\omega)\mathbf{I}$ , from deviatoric sources of wave excitation,  $\mathbf{M}_D(\omega)$ . The shallow depth of explosion sources makes an inversion for all six moment-tensor components ( $M_I(\omega)$  and the five independent elements of  $\mathbf{M}_D(\omega)$ ) difficult. Long-period surface waves, for example, are able to constrain only three components [Given and Mellman, 1986; Ekström and Richards, 1994]. In addition to  $m_{r\theta}$  and  $m_{r\phi}$ , poorly constrained since their Green's functions vanish for surface sources, an independent estimation of  $m_{rr}$  and  $m_{\theta\theta} + m_{\phi\phi}$  is difficult using only surface waves [Patton, 1988]. To overcome these limitations Patton [1988; 1991] performed moment-tensor inversions of regional observations from NTS explosions using both fundamental-mode and higher-mode surface waves. The higher-mode data provide additional constraints on the source, since Green's functions of  $m_{rr}$  and  $m_{\theta\theta} + m_{\phi\phi}$  differ substantially even for shallow sources for these waves.

An important goal of this study is to utilize our broad-band source recovery algorithms employing both surface-wave and body-wave data to determine  $M_I(\omega)$  and  $M_D(\omega)$  and to quantify the different contributions to  $M_D(\omega)$ , especially the tectonic release component,  $M_T(\omega)$ , whose contribution dominates the deviatoric component at low frequencies. Tectonic release contributes to source parameter estimates, such as the surface-wave magnitude  $M_s$  [e.g., Patton, 1991], and has the potential to bias both discriminants and minimum-yield detection maps, in particular when the amount of tectonic release is significant. A quantitative measure for the tectonic component is the "F factor", defined by Toksöz et al. [1964] as the ratio of the Rayleigh-wave amplitude generated by the explosion to that generated by the tectonic release. For a Poisson solid  $M_T/M_I \equiv 2/3F$  [Wallace, 1991].

The presence of a tectonic release component in seismic recordings from nuclear explosions, manifested in the presence of  $S_H$ -type seismic waves, has been recognized since the 1960s [Press and Archambeau, 1962; Brune and Pomeroy, 1963]. Models proposed for explaining the generation of  $S_H$ -type energy include explosion-triggered slip at preexisting, nearby faults [Aki and Tsai, 1972], release of tectonic prestress around the explosion source [Archambeau, 1972], and a combination of the two [Wallace, 1991]. Important unresolved questions associated with the tectonic release component are: (1) What is the scaling of the tectonic component with frequency? (2) Is there a change in the character of tectonic release with explosion yield/depth? (3) How does tectonic release vary in different geologic settings?

Most previous studies of tectonic release have focused on the Nevada Test Site [Aki and Tsai, 1972; Wallace et al., 1983; Wallace et al., 1985; Given and Mellman, 1986; Patton, 1988] and the Shagan River, Kazakhstan nuclear test site [Helle and Rygg, 1984; Given and Mellman, 1986; Walter and Patton, 1990; Ekström and Richards, 1994], while little attention has been devoted to investigating the tectonic component from nuclear tests near Lop Nor, China [Zhang, 1996].

Furthermore, most studies have utilized either surface waves [e.g., Given and Mellman, 1986; Ekström and Richards, 1994; Zhang, 1996] or body waves [Wallace et al., 1983; Wallace et al., 1985] alone, making a broad-band estimate of  $M(\omega)$  difficult. Therefore, the variation of  $F$  with frequency has received little attention, although scarcity of high-frequency  $S_H$  waves indicates that it decreases with frequency. Our approach based on a broad-band source recovery will allow us to constrain this quantity and improve our physical understanding of explosion source processes.

Another important question concerns the scaling of tectonic release for different explosions. Some authors have suggested, for example, that  $F$  decreases with time for explosions detonated in close proximity to each other [Aki and Tsai, 1972; Wallace, 1991], and that it is affected by other factors such as explosion yield and depth of burial [Aki and Tsai, 1972]. From a moment-

tensor inversion of 16 explosions on Pahute Mesa, Patton [1991] concluded that the character of the tectonic component changes with explosion yield, going from vertical strike-slip mechanisms to dip-slip reverse faulting at yields of about 200-300 kT. Since  $M_s$  is biased high (low) for strike-slip (thrust) mechanisms [Patton, 1980], it is important to test this hypothesis at other nuclear test sites.

In this study, we consider explosions from the Chinese nuclear test site at Lop Nor. We have collected a large number of broad-band and long-period three-component seismograms at regional and teleseismic distances for several nuclear tests from 1990-1996 spanning a range of sizes. Applying our broad-band source recovery algorithms to this data set, we will be able to improve our physical understanding of the processes affecting seismic wave excitation from explosion sources. Gaining new insights into how tectonic release scales with frequency and explosion yield/depth should also lead to a better understanding on how high-frequency discriminants such as  $P/L_g$  are affected by tectonic release.

Recovering broad-band estimates of the source-time function from seismic data at regional and teleseismic distances is a difficult inverse problem, requiring precise corrections for deterministic propagation effects and careful averaging procedures to reduce stochastic fluctuations due to non-deterministic scattering. Our approach is based on techniques developed by Jordan and coworkers for determining earthquake source-time functions. In particular, we adapt waveform isolation and analysis tools developed by *Gee and Jordan* [1992] and *Ihmlé and Jordan* [1995], which use synthetic seismograms to improve the localization of signal measurements in both time and frequency domains. We proceed as follows:

- (1) For each observed seismogram  $s_j(t)$  ( $j$  = station index), we generate six Green's function seismograms  $\tilde{g}_j^k(t)$  ( $k$  = component index;  $k \in [rr, \theta\theta, \phi\phi, r\theta, r\phi, \theta\phi]$ ) from the best available structural model. At teleseismic distances, we use a global tomographic model, such as the Preliminary Reference Earth Model (PREM) of Dziewonski and Anderson [1981] in conjunction with the degree-12 structure S12\_WM13 of Su et al. [1994]. Using Green's functions calculated for an aspherical earth model reduces contamination due to propagation effects and enables us to obtain a clearer image of the source. For the work at regional distances, we adopt appropriate path-averaged models [e.g., *Gaherty and Jordan*, 1995], where available. We use an iterative inversion algorithm to determine a source mechanism,  $\mathbf{m}(\omega)$ , from a series of narrow-band filtered cross-correlations between  $s_j(t)$  and  $\tilde{g}_j^k(t)$ . ( $\mathbf{m}(\omega)$  is the isomorphic equivalent of the symmetric tensor  $\mathbf{M}(\omega)$  [Silver and Jordan, 1982].)



- (2) Using an average source mechanism,  $\hat{\mathbf{m}} = \mathbf{m}(\omega_0)$ , we generate synthetic seismograms  $\tilde{s}_j(t) = \tilde{\mathbf{g}}_j(t) \cdot \hat{\mathbf{m}}$  assuming that the source is a step-function at  $t_0$ .
- (3) Using the isolation-filtering procedures detailed by Gee and Jordan [1992], we extract two functions of frequency, an amplitude ratio  $A_j(\omega) / \tilde{A}_j(\omega)$  and a differential phase delay  $\Delta t_j(\omega) = t_j(\omega) - \tilde{t}_j(\omega)$ , from individual waveforms on  $s_j(t)$ . At teleseismic distances, the waveforms we analyze typically include the  $P$  and  $S$  body phases and the  $R_1$  and  $G_1$  surface waves. Corrections are applied to account for the amplitude and phase distortions due to the time- and frequency-localization operations intrinsic to the analysis [Gee and Jordan, 1992].
- (4) We average  $\Delta t_j(\omega)$  and the logarithm of  $A_j(\omega) / \tilde{A}_j(\omega)$  over the network from which we obtain estimates of  $\Delta t(\omega)$  and  $A(\omega)$ . Note that averaging is *not* done over the complex spectrum,  $f(\omega)$ ; if it were, the small phase delays associated with unmodeled propagation effects would cause destructive interference among the signals, and therefore lead to amplitude bias.
- (5) We invert the estimates of  $A(\omega)$  and  $\Delta t(\omega)$  for  $f(t)$ , subject to an appropriate set of smoothing constraints and functional bounds.

## Research Accomplishments

Modifications to the Analysis Procedures. We have adapted our algorithms to synthesize broadband amplitude and phase-delay estimates from regional and teleseismic data, developed in the context of our research on earthquake source mechanisms [Ihmlé *et al.*, 1993; Ihmlé and Jordan, 1994], to inversions of explosion sources. In our previous earthquake studies, we have assumed that the source-time function is non-negative. Physically, this is a statement that there is no backslip in the fault. The mathematical advantage of this assumption is that a lower bound is imposed on the inversion for  $f(t)$ , which constrains the solution by reducing the size of the model space [Ihmlé and Jordan, 1994]. This assumption is not generally valid for nuclear explosions, because many of them are observed to have overshoot, which means that  $f(t)$  becomes negative over some time interval of the source. However, when inverting for the deviatoric (tectonic) component of the source-time function,  $f_D(t)$ , non-negativity should be a good first-order approximation. Another constraint commonly applied to earthquake moment tensor inversions is to require the moment tensor to be deviatoric. Such a constraint is clearly inappropriate when inverting for a moment tensor that is composed of both explosion and deviatoric components. A further difficulty encountered when inverting for explosion source mechanisms is due to the fact that the depth of moment release is very close to the earth's

surface. At shallow depths the Green's functions  $\tilde{g}^{r\theta}(t)$  and  $\tilde{g}^{r\phi}(t)$  almost vanish, since the normal component of the stress tensor is zero at the free surface. This means that  $m_{r\theta}$  and  $m_{r\phi}$  cannot be well constrained. A common practice in source inversions of nuclear explosions and shallow earthquakes is to simply set these two components equal to zero [Kanamori and Given, 1981; Given and Mellman, 1986]. However, this procedure is adequate only for narrow-band moment-tensor inversions, since the sensitivity to shallow structure becomes larger with increasing frequencies, which leads to high-frequency moment-tensor solutions that are biased with respect to the low-frequency inversions when  $m_{r\theta} = m_{r\phi} = 0$  is assumed. We overcome this problem by recasting the inverse problem using a projection operator,  $\mathbf{P}_s = \mathbf{I} - \tilde{\mathbf{g}}_s \tilde{\mathbf{g}}_s^\dagger$ . This operator annihilates any possible information on  $m_{r\theta}$  and  $m_{r\phi}$  contained in the Green's functions  $\tilde{\mathbf{g}}$  or in the data  $\mathbf{s}$ . This modifies the inverse problem from:

$$\tilde{\mathbf{g}} \cdot \hat{\mathbf{m}} = \tilde{\mathbf{g}}_d \cdot [m_{rr}, m_{\theta\theta}, m_{\phi\phi}, m_{\theta\phi}] + \tilde{\mathbf{g}}_s \cdot [m_{r\theta}, m_{r\phi}] = \mathbf{s} \quad (1)$$

to

$$\mathbf{P}_s \tilde{\mathbf{g}} \cdot \hat{\mathbf{m}} = \mathbf{P}_s \mathbf{s},$$

and allows a recovery of the moment tensor over a broad frequency range. Another advantage of the projection operator approach is that it allows a self-consistent error analysis, since the posterior model covariance matrix will reflect the constraints used in obtaining the solution.

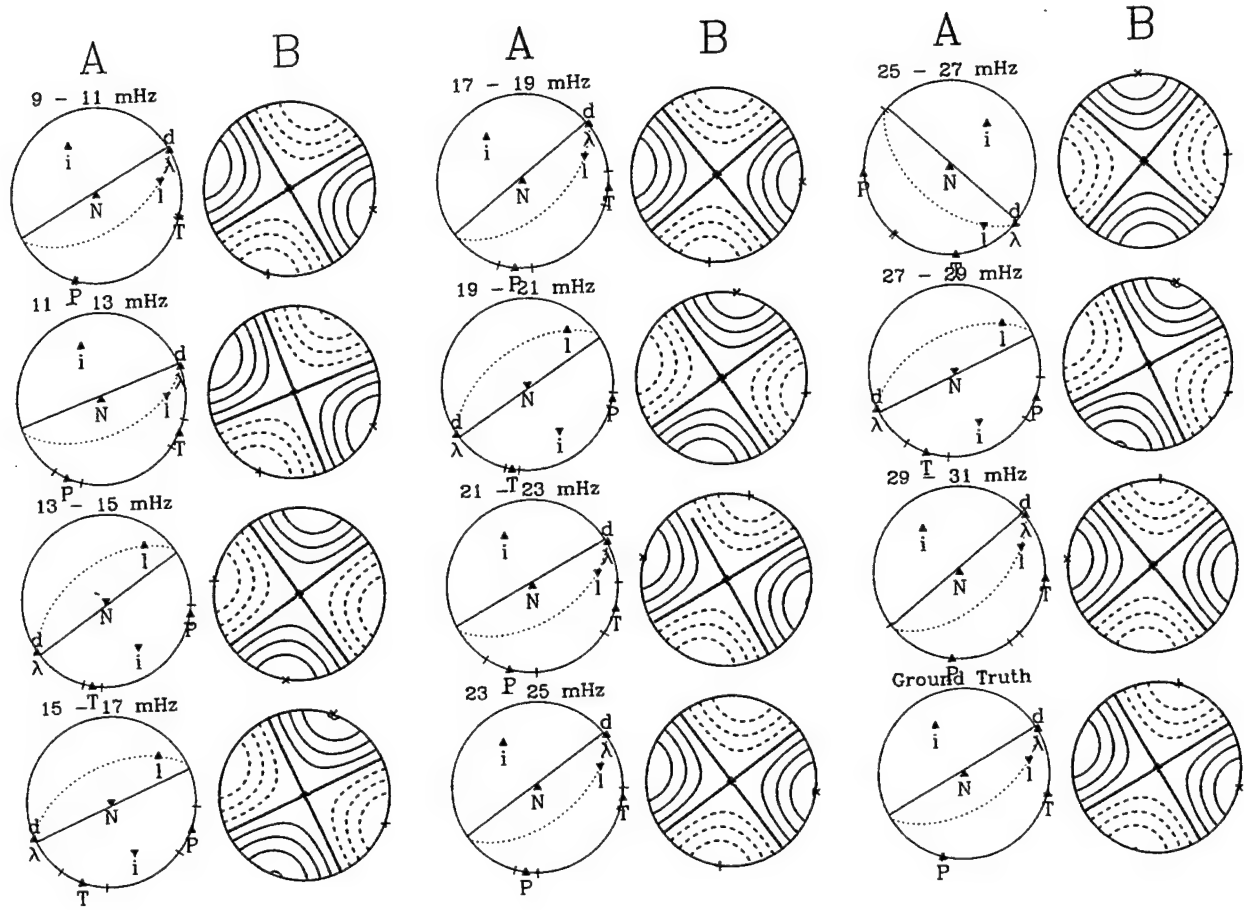
Our formalism for obtaining the source mechanism is based on determining the elements of the moment tensor directly. This contrasts with methodologies that formulate the Green's functions using three fundamental faults [Kanamori and Given, 1981] plus an explosion source [Given and Mellman, 1986]. We also do not impose any a priori constraint on the fault geometry or even require the deviatoric component to be a double couple.

Synthetic Test Case. To examine the performance of our algorithms we construct the following test case. Using a fictitious source located at the Lop Nor test site with a moment tensor composed of an isotropic part plus a deviatoric mechanism with identical scalar moment, we calculate 3-D synthetic seismograms for a PREM plus S12\_WM13 earth structure for 20 IRIS and Geoscope stations at regional and teleseismic distances to simulate the data. The aspherical synthetics are calculated employing the asymptotic formalism of Woodhouse and Dziewonski [1984]. The deviatoric moment tensor is the Harvard-CMT solution of the 94/9/7 event in Southern Xinjiang, China (a predominantly strike-slip earthquake with a small CLVD component and a scalar moment of  $7.7 \times 10^{16}$  Nm) mimicking the tectonic release component. Green's functions are calculated for the 1-D PREM model. Our imprecise knowledge of 3-D earth structure is a primary source of signal-generated noise which makes an inversion for the source-time function difficult. Using 3-D synthetics as data and 1-D Green's functions provides

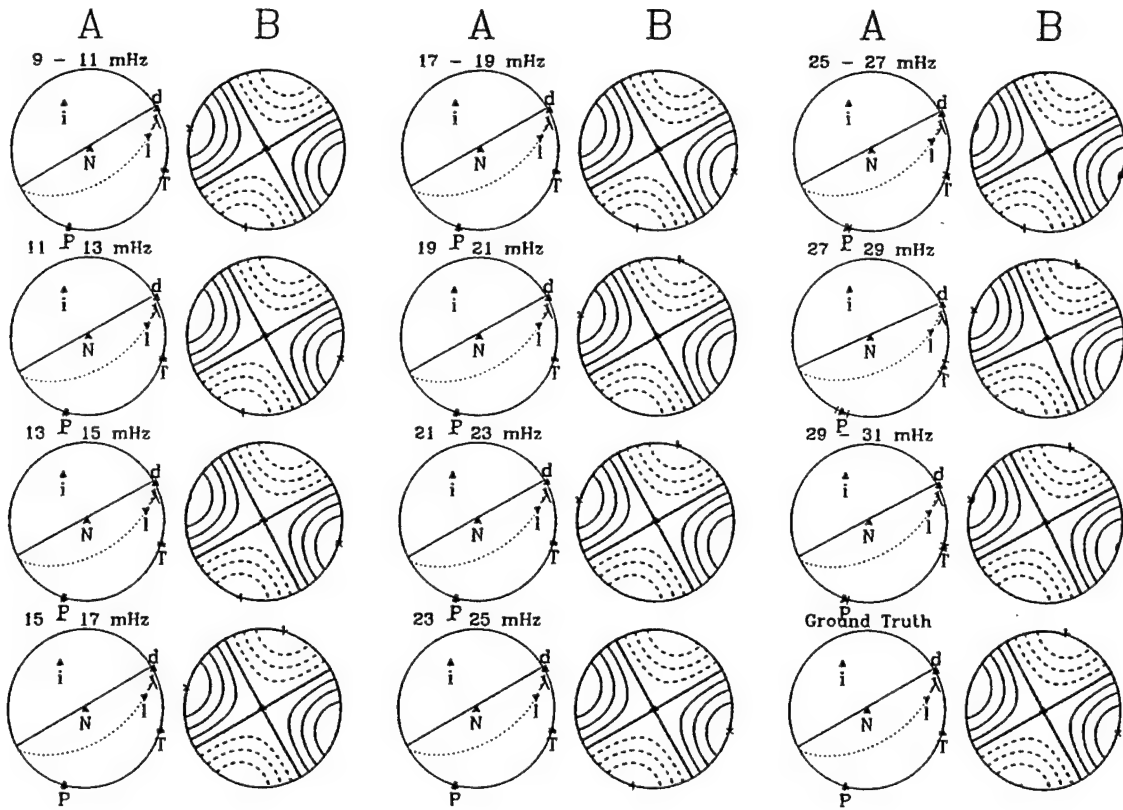
a proxy for difficulties encountered with real data. Since the explosion source is located at shallow depth (1 km), the  $m_{r\theta}$  and  $m_{r\phi}$  components of the moment tensor are ill-constrained; we therefore project out these components using the algorithm outlined above. Utilizing the fact that transverse-component (LHT) seismograms do not contain any energy from a purely isotropic source our moment-tensor inversion proceeds in two steps. First, we invert the LHT seismograms and obtain an estimate for the tectonic release. Second, we invert the vertical-component data, which yields a moment tensor that is a combination of the isotropic component plus the tectonic release.

Figure 1 shows the results of the initial moment-tensor inversion using long-period, minor-arc Love waves recorded on the transverse component. We apply a series of narrow-band filters to the broad-band cross-correlation function and obtain independent moment-tensor solutions  $\mathbf{M}_D(\omega)$  for each frequency band. The source mechanism plots are constructed using the methodology described by *Riedesel and Jordan [1989]*. Column A displays the three principal axes of the source mechanism (**T**, **N**, **P**) together with the unit mechanism vector ( $\hat{\lambda}$ ) and the canonical unit vectors  $\hat{\mathbf{d}}$ ,  $\hat{\mathbf{i}}$ , and  $\hat{\mathbf{i}}$ , representing a pure double couple, a compensated linear vector dipole, and a pure dilatation, respectively. The contours of the P-wave first motion are shown in column B. This approach provides a comprehensive visualization of the source mechanism. In particular, it is possible to directly assess the uncertainties in the source mechanism and quantify the contribution of an isotropic component, a very useful feature when investigating non-deviatoric sources (see below). While all solutions are strike-slip mechanisms, the source mechanisms vary rapidly between adjacent frequency bands and differ from the projected ground-truth mechanism (bottom right). This instability in the inversion is primarily a result of mapping phase-shifts due to unmodeled lateral heterogeneities along the propagation path into the source mechanism. To account for these propagation effects we iterate our inversion by (1) calculating the phase-shifts between data and synthetics (computed from a moment tensor obtained in the initial inversion), (2) phase-shifting the Green's functions, and (3) reinverting for  $\mathbf{M}_D(\omega)$ . The results depicted in Figure 2 document the success of this methodology. The agreement between different frequency bands and with the projected ground-truth moment tensor is excellent.

Horizontally polarized shear waves provide additional constraints on  $\mathbf{M}_D(\omega)$  and are less contaminated by shallow heterogeneity than surface waves. Figure 3 shows the results of the moment-tensor inversion using  $S_H$  waves, adjusted for the phase-shifts due to aspherical heterogeneities. The agreement with the Love-wave solutions is good, and indicates that the two data sets can be used to cross-check the inversion results and provide a broad frequency band.



**Figure 1.** Source mechanism plots (A) and initial  $P$ -wave radiation patterns (B) for  $M_D(\omega)$  in 2 mHz frequency bands ranging from 9 to 31 mHz plotted using equal area projection. On each plot (A), the three principal axes  $\hat{e}_1$ ,  $\hat{e}_2$ ,  $\hat{e}_3$  (eigenvectors of  $M_D(\omega)$ ) corresponding to eigenvalues  $\lambda_1 \geq \lambda_2 \geq \lambda_3$ , are plotted as T, N, and P on the lower focal hemisphere. The mechanism is characterized by the unit vector  $\hat{\lambda} = \sum \lambda_i \hat{e}_i$ , which can be compared with the canonical unit vectors  $\hat{d}$ ,  $\hat{l}$ , and  $\hat{i}$ , representing a pure double couple, a pure compensated linear vector dipole, and a pure dilatation, respectively. The dashed line shows the locus of all deviatoric mechanisms. Vectors are plotted as downward pointing filled triangles if they are on the lower focal hemisphere and as upward pointing if they are projected from the upper hemisphere. For a pure double couple the axes T, N, and P are the tension, neutral, and compression axes, respectively. The contours of the  $P$ -wave first motion are shown in (B). Solid (dashed) contours denote compressional (dilatational) first motion, thick contours are nodal lines. Initial moment-tensor inversion results using first-orbit, transverse-component Love wave-forms from a synthetic test case. "Data" seismograms are calculated using PREM plus the 3D model S12\_WM13. Green's functions are calculated for the 1D PREM model. The  $m_{r\theta}$  and  $m_{r\phi}$  components are projected out from both solution and data space. The moment tensor is constrained to be deviatoric. For comparison, the projected input moment tensor ("Ground Truth") is shown on the lower right.



**Figure 2.** Mechanism plots (A) and  $P$ -wave radiation patterns (B) from the Love-wave inversion (phase-aligned) for the test case described in Figure 1. Prior to performing the moment-tensor inversions, a phase-shift,  $\Delta t_j(\omega)$ , is calculated for each seismogram in each frequency band using a preliminary  $\hat{\mathbf{M}}_D$  from the initial moment-tensor inversion (Figure 1). The Green's functions are phase-shifted by  $\Delta t_j(\omega)$  and a new inversion for  $\mathbf{M}_D(\omega)$  is performed. The agreement between the frequency bands and with the projected ground-truth moment tensor is remarkable.

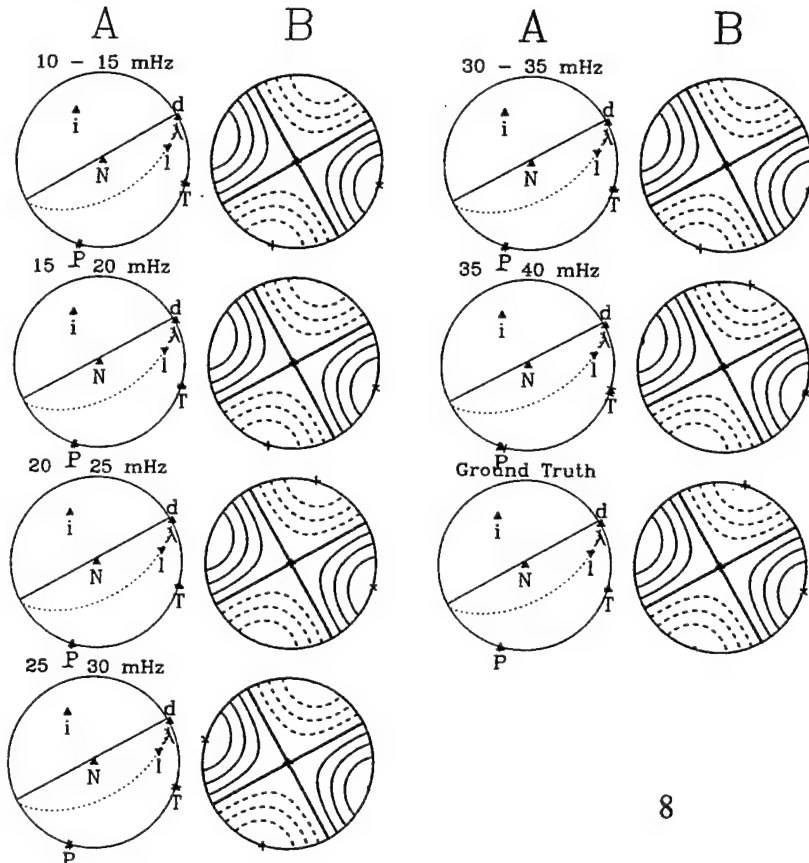


**Figure 3.** Mechanism plots (A) and  $P$ -wave radiation patterns (B) from the moment-tensor inversion (after phase alignment) using  $S_H$  waveforms for the same test case described in Figure 1. The  $m_{r\theta}$  and  $m_{r\phi}$  components are projected out and the moment tensor is constrained to be deviatoric. Results from the body-wave inversions agree very well with the surface-wave results displayed in Figure 2.

Network-averaged amplitudes,  $A(\omega)/\tilde{A}(\omega)$ , and time-shifts,  $\Delta t(\omega)$ , for the  $S_H$  waves obtained from cross-correlations of data and synthetics (using an average moment tensor from Figure 3) are displayed in Figure 4. The small residuals ( $A(\omega)/\tilde{A}(\omega) \approx 1$  and  $\Delta t(\omega) \approx 0$ ) are further proof of the success of the moment-tensor inversion. The residual time shifts in Figure 4, are due to 3D propagation effects not removed by the network average. Using these amplitude and time shift spectra we can invert for the source-time function.

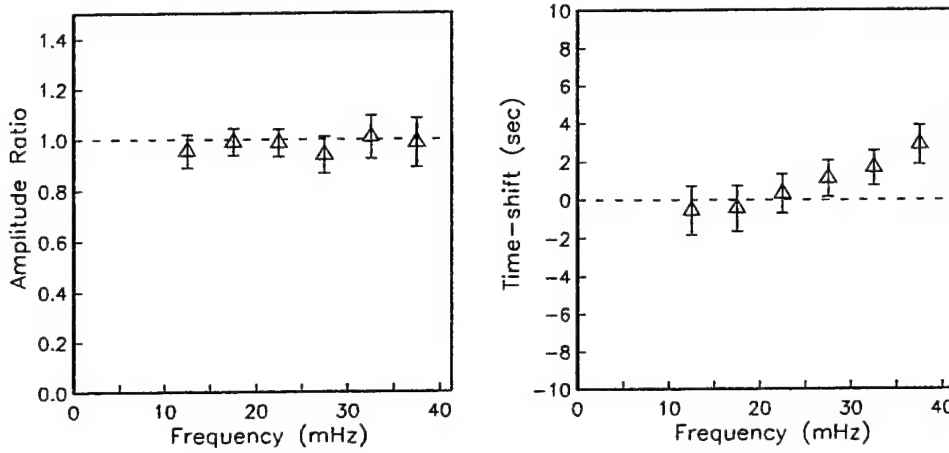
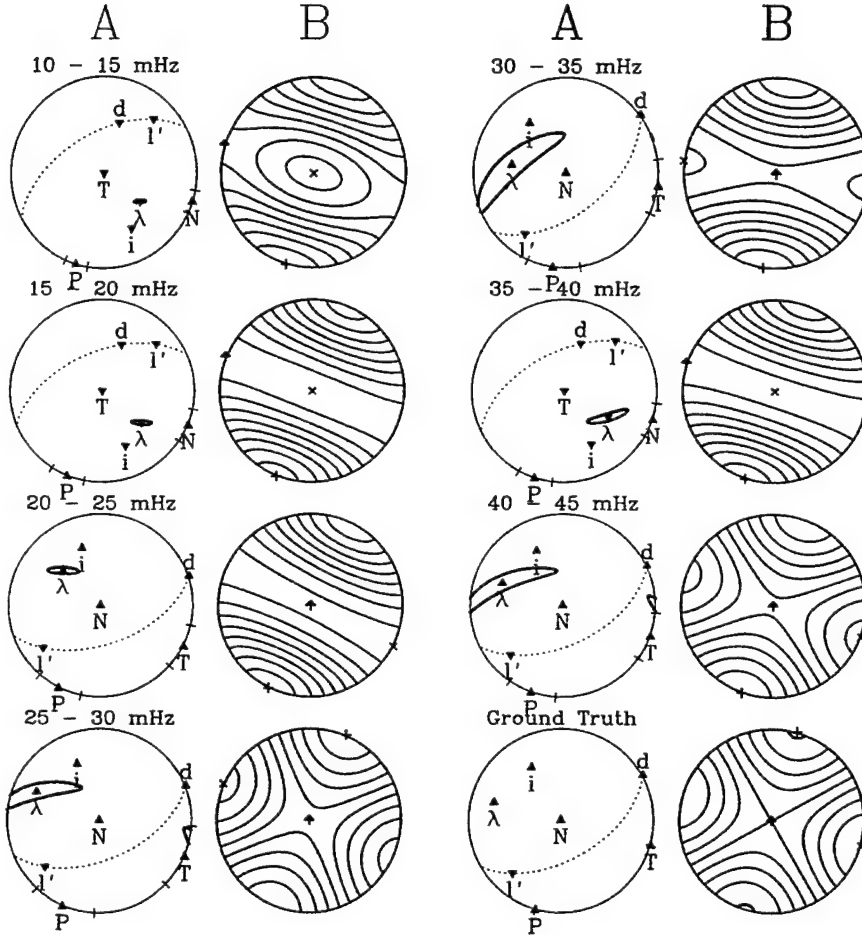


**Figure 4.** Network-averaged amplitude ratios,  $A(\omega)/\tilde{A}(\omega)$ , and time-shifts,  $\Delta t(\omega)$ , measured from narrow-band cross-correlations of  $S_H$  waveforms using an average moment tensor  $\hat{\mathbf{M}}_D$  from Figure 3. Agreement between data and synthetics indicates the success of the moment-tensor inversion. Residual time shifts are due to 3D propagation effects not removed by the network average.

Transverse-component data do not constrain  $m_{rr}$  (since the corresponding Green's function,  $\tilde{g}^{rr}(t)$ , is zero for a spherically symmetric earth). Furthermore,  $\tilde{g}^{\theta\theta}(t) = -\tilde{g}^{\phi\phi}(t)$ , which results in  $m_{\theta\theta} = -m_{\phi\phi}$ . The LHT inversion, therefore, always recovers a double-couple, vertical strike-slip source. However, since  $m_{rr}$  is unconstrained it is possible to fit the LHT data equally well with an alternative source mechanism, the one corresponding to a 45° dip-slip fault with a strike rotated by 45° and a scalar moment twice that of the strike-slip source [e.g., *Aki and Richards*, 1980]. To resolve this ambiguity in  $\mathbf{M}_D(\omega)$  and to recover  $\mathbf{M}_I(\omega)$  we apply our inversion procedure to the body-wave portion between  $P$  and the minor-arc Rayleigh waves ( $R_1$ ) on vertical-component recordings. We calculate synthetic test data using the S12\_WM13 3D earth model and a moment tensor  $\mathbf{M} = M_I \mathbf{I} + M_D \hat{\mathbf{M}}_D$ , with  $M_D/M_I = 1$  and  $\mathbf{M}_D$  from above. The inversion allows for a non-zero isotropic component; however,  $m_{r\theta}$  and  $m_{r\phi}$  are projected out. Figure 5 shows  $\mathbf{M}(\omega)$  between 10 and 45 mHz. Displaying the source mechanism unit vector,  $\hat{\lambda}$ , together with the canonical double couple, CLVD, and isotropic vectors makes it particularly easy to assess the contribution of the purely dilatational component. The angular distance

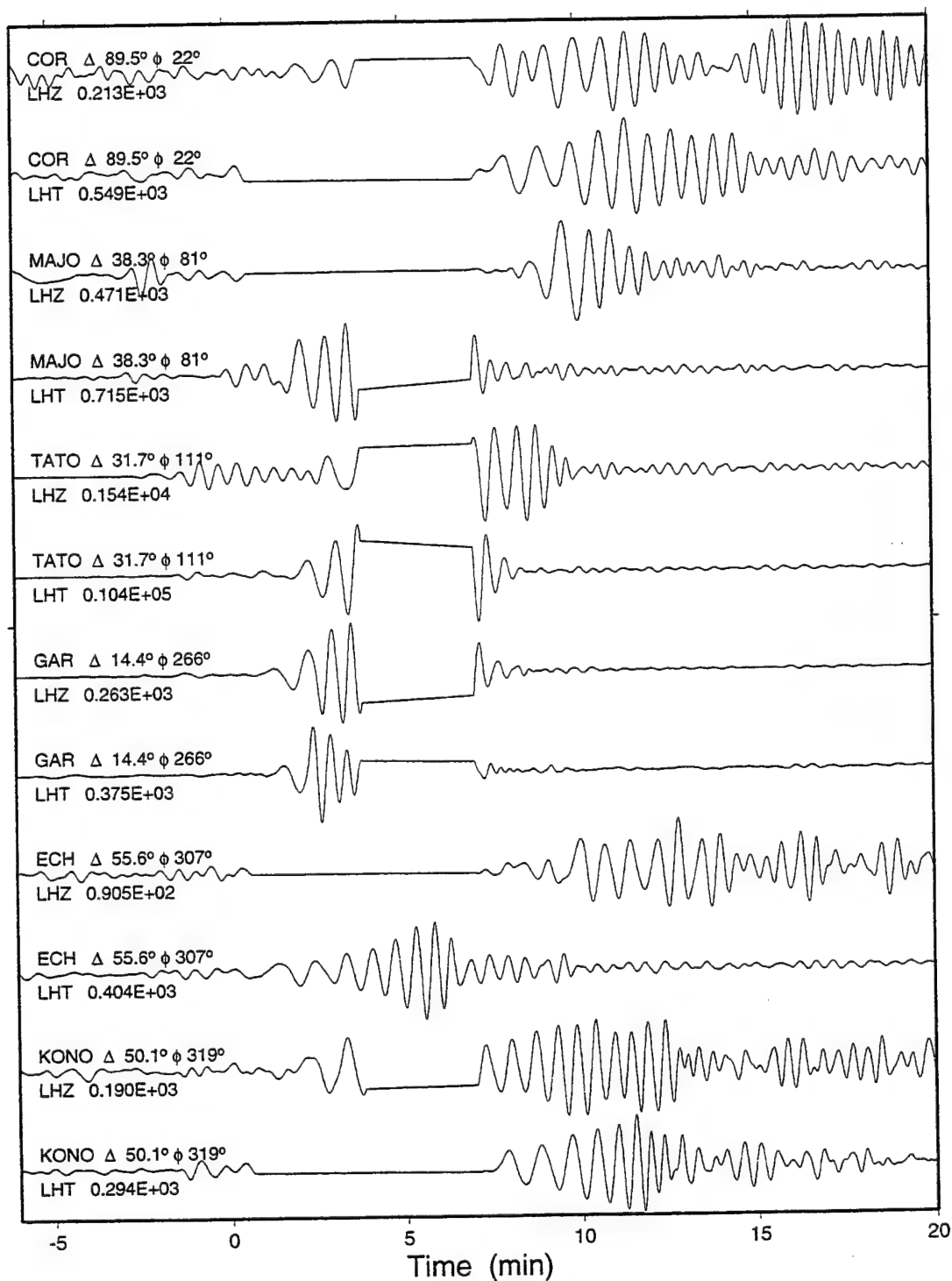


between  $\hat{\lambda}$  and  $\hat{i}$  measures the deviation from an isotropic source. This is the first time that the *Riedesel and Jordan* [1989] formalism has been applied to assess and display significantly non-deviatoric mechanisms. The agreement between different frequency bands and with the known solution (lower right), although not as good as for the transverse-component data, is still rather remarkable. These synthetic tests indicate that we can recover both deviatoric and isotropic source mechanisms from vertical-component and transverse-component data.



**Figure 5.** Mechanism plots (A) and  $P$ -wave radiation patterns (B) from the (phase-aligned) moment-tensor inversion using the body-wave portion of vertical-component records arriving prior to  $R_1$ . Uncertainties in the mechanism vectors are depicted by 95% confidence ellipses (heavy lines). The projected input moment tensor (ground truth) consists of both isotropic,  $M_I \mathbf{I}$ , and deviatoric,  $M_D \hat{\mathbf{M}}_D$ , components ( $M_D/M_I = 1$ ) and is displayed on the bottom right. Data and synthetics are calculated for the same models as in Figure 1. The inversion is performed with  $m_{r\theta}$  and  $m_{r\phi}$  components projected out; the moment tensor is no longer constrained to be deviatoric.

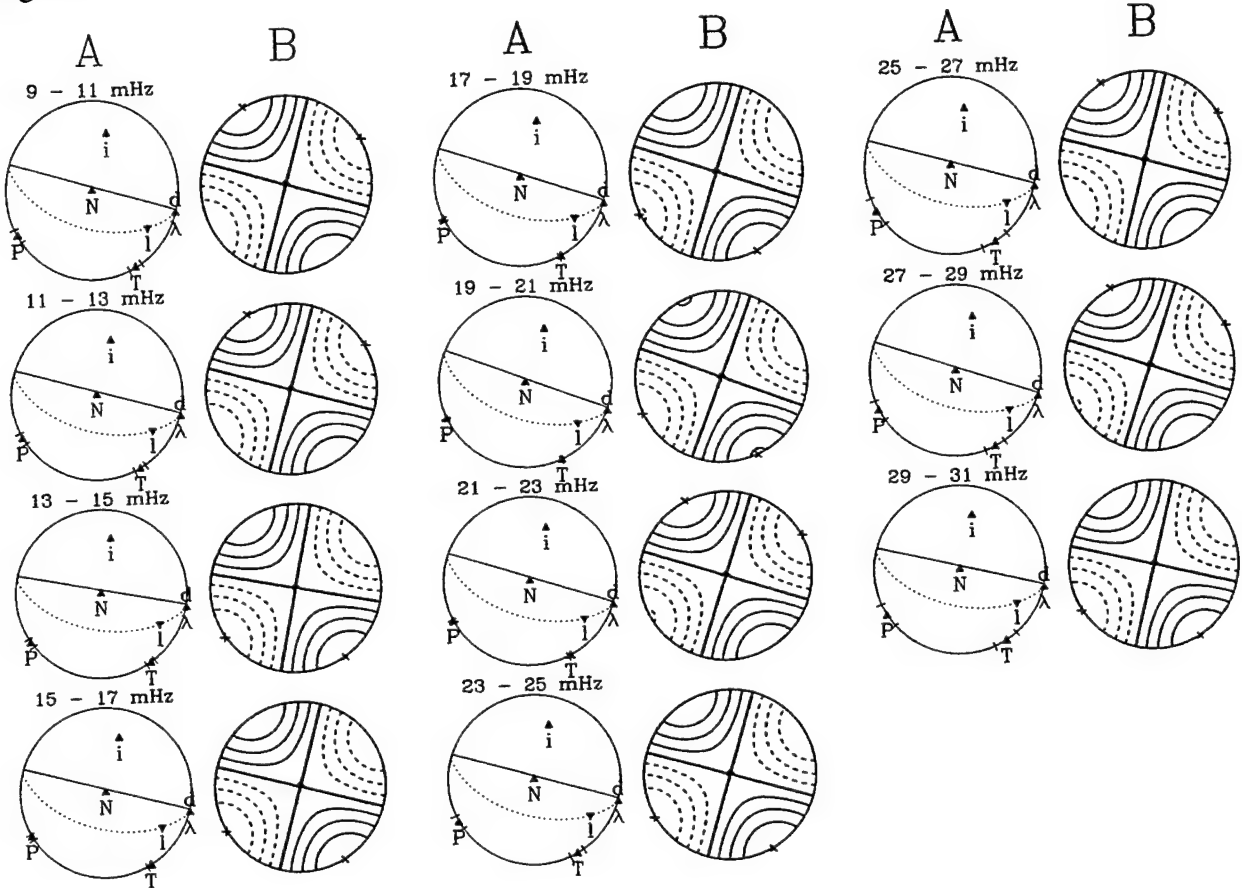
Lop Nor Nuclear Test from 92/5/21. Having established the performance of our moment-tensor recovery methodology on a synthetic example, we next apply our algorithms to data from the Chinese nuclear test conducted on 92/5/21. While this is the largest Chinese nuclear test to date, the station coverage provided by the IRIS and Geoscope networks, is sparse by today's standards. Love waves are clearly identifiable on the LHT recordings from this event and are of equal or larger amplitude than the Rayleigh waves (Figure 6), demonstrating that a significant component of tectonic release is present.



**Figure 6.** Vertical-component Rayleigh-wave and transverse component Love-wave seismograms for six stations at varying epicentral distance,  $\Delta$ , and source-receiver azimuth,  $\phi$ , from the 92/5/21 Chinese nuclear test near Lop Nor. Seismograms are band-pass filtered with a six-pole Butterworth filter (corners at 8.5 and 31.5 mHz). Traces are aligned on the theoretical Love wave arrival time; maximum trace amplitude is displayed below the individual traces.



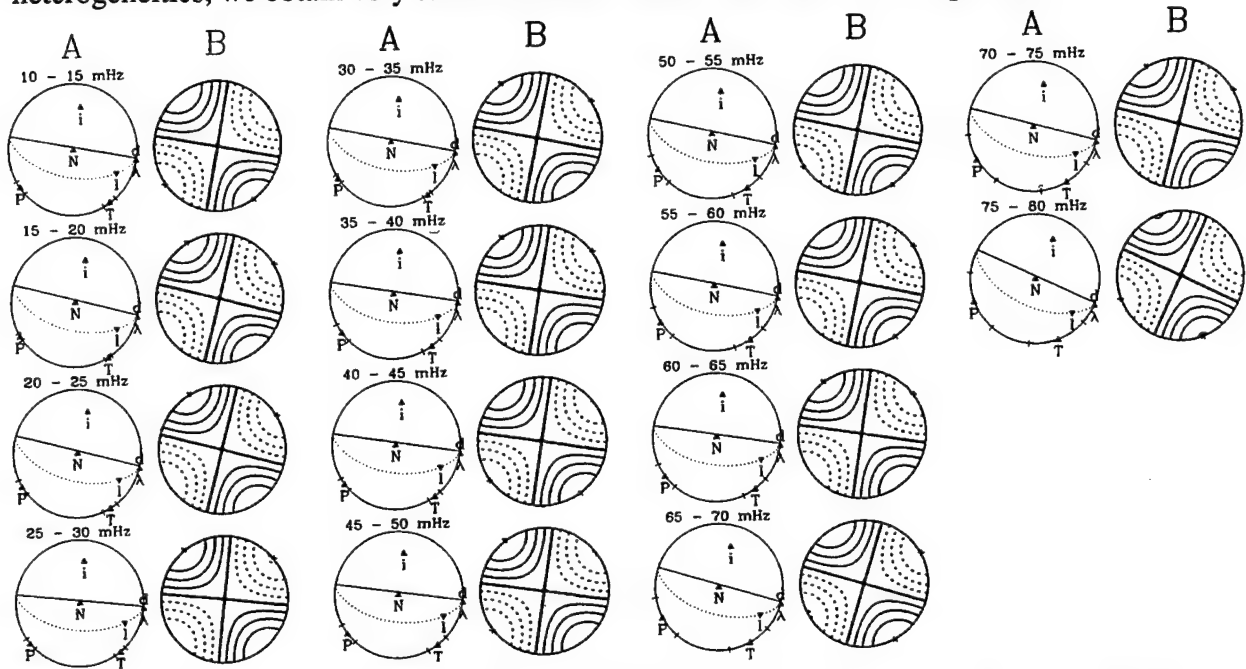
Using the same analysis procedure as above, we invert these data traces for the deviatoric moment tensor. However, we utilize our knowledge of long-wavelength aspherical earth structure to calculate 3-D Green's functions using PREM together with the 3-D model S12\_WM13. Figure 7 displays the inversion results using transverse-component, first-orbit Love waves ( $G_1$ ). The resulting moment tensor,  $\mathbf{M}_D(\omega)$ , is a strike-slip mechanism which shows little variation between frequency bands, with the strike of the faults plane varying only by a few degrees.



**Figure 7.** Mechanism plots (A) and  $P$ -wave radiation patterns (B) from the (phase-aligned) Love-wave inversion for the 92/5/21 nuclear test near Lop Nor, China. The analysis procedure is the same as for the synthetic test case described earlier, except that we calculate Green's function seismograms for the aspherical model S12\_WM13. The resulting moment tensor,  $\mathbf{M}_D(\omega)$  remains unchanged across the entire frequency band.

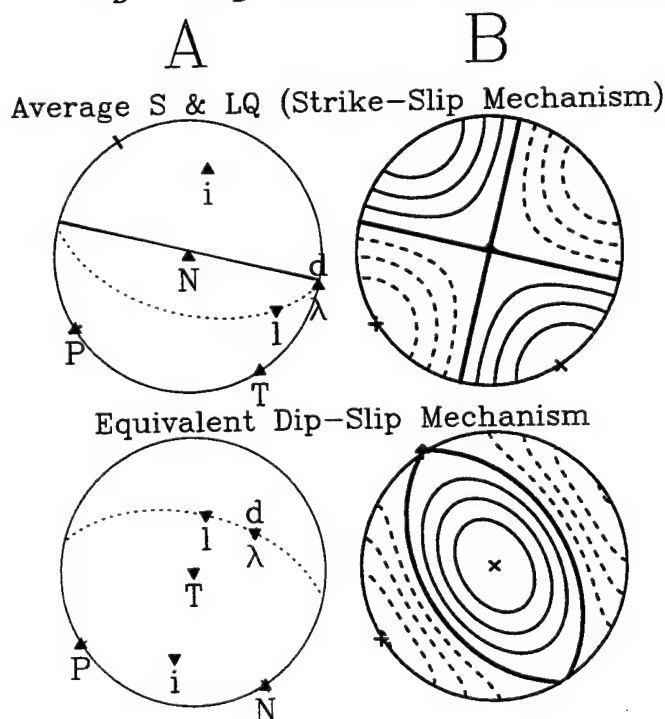
This event also generated  $S_H$  waves clearly observable at several stations at regional and teleseismic distances. Inverting these shear waves for  $\mathbf{M}_D(\omega)$  yields results consistent with the

Love-wave inversion (Figure 8). Since the  $S$  waves are less influenced by strong, near-surface heterogeneities, we obtain very stable inversion results from 100 s to 12 s period.



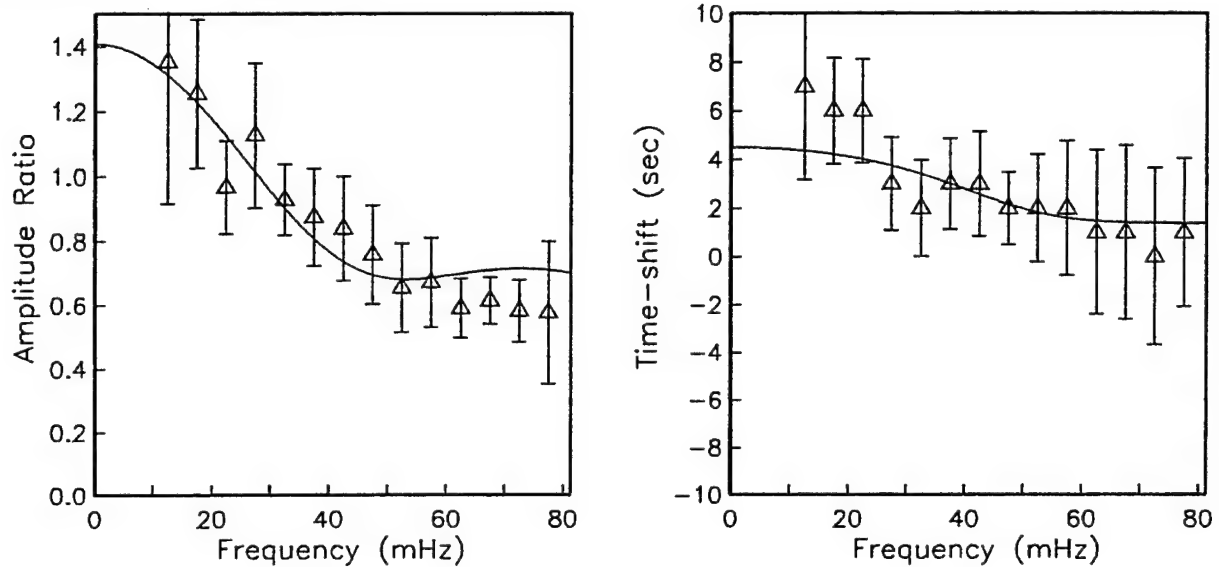
**Figure 8.** Mechanism plots (A) and  $P$ -wave radiation patterns (B) from the inversion of phase-aligned  $S_H$  waveforms for the 92/5/21 nuclear explosion near Lop Nor, China. The resulting moment tensor,  $M_D(\omega)$ , is nearly identical to that obtained from the Love-wave inversion.

Figure 9 depicts the source mechanism averaged over all frequency bands from the  $G_1$  and  $S_H$  inversion. Also shown is the dip-slip mechanism that satisfies the data equally well. The scalar moments of these two mechanisms are,  $M_D^{SS} = 0.85 \pm 0.05 \times 10^{17}$  Nm and  $M_D^{DS} = 2M_D^{SS} = 1.7 \pm 0.1 \times 10^{17}$  Nm, respectively.



**Figure 9.** Mechanism plots (A) and  $P$ -wave radiation patterns (B) averaged over all frequency bands from the Love-wave and  $S_H$  inversions. Due to the ambiguity intrinsic in inverting transverse-component data, both vertical strike-slip and dip-slip mechanisms satisfy the data equally well.

The network-averaged amplitude and time-shift spectra for the  $S_H$  waves using the average moment tensor are shown in Figure 10. While the absolute amplitude is uncertain within a factor two, owing to the ambiguity between strike-slip and dip-slip mechanisms, the amplitude spectral roll-off suggests a decrease in the size of the tectonic component, as long as the source mechanism does not change from dip-slip to strike-slip between 0.01 and 0.08 Hz. The time shifts at low frequencies ( $\Delta t(\omega) \cong 4\text{--}7$  s) indicate a centroid time more appropriate for an earthquake than an explosion.



**Figure 10.** Network-averaged amplitude ratios,  $A(\omega)/\bar{A}(\omega)$ , and time-shifts,  $\Delta t(\omega)$ , (triangles with 1- $\sigma$  standard errors) measured from narrow-band cross-correlations of  $S_H$  waveforms using an average moment tensor  $\bar{\mathbf{M}}_D$  from Figure 9. The solid lines indicate the data fit obtained from the source-time function displayed in Figure 11.

Figure 11 depicts the source-time function associated with the deviatoric mechanism,  $f_D(t)$ , obtained from a constrained inversion of the network-averaged amplitude and time-shift spectra. The inversion is performed using a quadratic programming approach that allows for smoothness constraints and one-sided constraints [Ihmlé *et al.*, 1993]. To limit the size of the solution space, we constrain  $f_D(t)$  to be non-negative. The source-time function shows some complexity, with a sharp pulse in moment release followed by a long, smooth tail (Figure 2f). Although we must still examine potential sources of bias, we hypothesize that the pulse-like component is caused by scattering of energy from the explosion into  $S_H$ -polarized waves, perhaps by near-source lateral structure, and the smoothly varying component is earthquake-like radiation due to tectonic release. If correct, this interpretation would favor a tectonic release model where the explosion

triggers slip at nearby faults [Aki and Tsai, 1972] over the shatter-zone model advocated by Archambeau [1972].

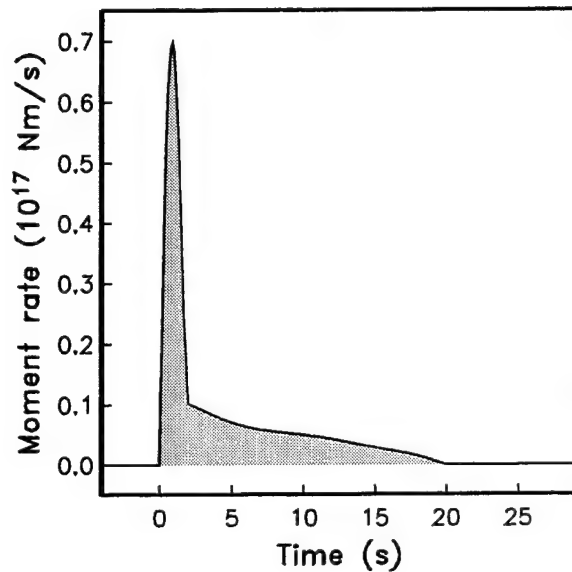


**Figure 11.** Source-time function,  $f_D(t)$ , obtained from a constrained inversion of the network-averaged amplitudes and time-shifts depicted in Figure 10. Although not unique, the source-time function provides a good spectral fit. The pulse-like component is hypothesized to be due to scattering of explosion energy, while the smoothly varying component, comprising about 60% of the total moment, can be explained by tectonic release. The moment-rate is scaled assuming a dip-slip mechanism.

To recover the complete moment tensor  $\mathbf{M}(\omega) = \mathbf{M}_I(\omega) + \mathbf{M}_D(\omega)$  and to discriminate between the two candidate mechanisms obtained from inverting the  $S_H$ -type data, we use the vertical-component data. We perform separate inversion using (1) first-orbit Rayleigh waves and (2) the body-wave portion between  $P$  and  $R_1$ . The Rayleigh-wave inversions reveal the presence of a strong isotropic component to the source mechanism,  $\hat{\lambda}$ , evident by the small angular distance between  $\hat{\lambda}$  and  $\hat{\mathbf{i}}$  (Figure 12). With a few exceptions the inversions are stable across the entire frequency range. The mechanism uncertainties, quantified by the 95% confidence ellipses, illustrate a trade-off between isotropic and CLVD mechanisms. Rayleigh waves are unable to differentiate between an isotropic component and a vertical CLVD,  $\hat{\mathbf{i}}'$ , corresponding to horizontal extension and vertical compression.

The body-wave data includes various phases ( $P$ ,  $S$ ,  $pP$ ,  $pS$ ,  $sS$ ,  $sP$ , etc.), leaving the source at different take-off angles, thus providing good constraints on the source mechanism. We exclude higher-mode surface waves that show a strong contamination due to near-surface heterogeneities. Body-wave phases turning in the mantle are less affected by shallow structure than surface waves, and should therefore allow us to improve on the Rayleigh-wave moment-tensor estimates. Indeed, the body-wave inversions show consistency between  $\mathbf{M}(\omega)$  determined in different frequency bands and compare well with the Rayleigh-wave results (Figure 13).

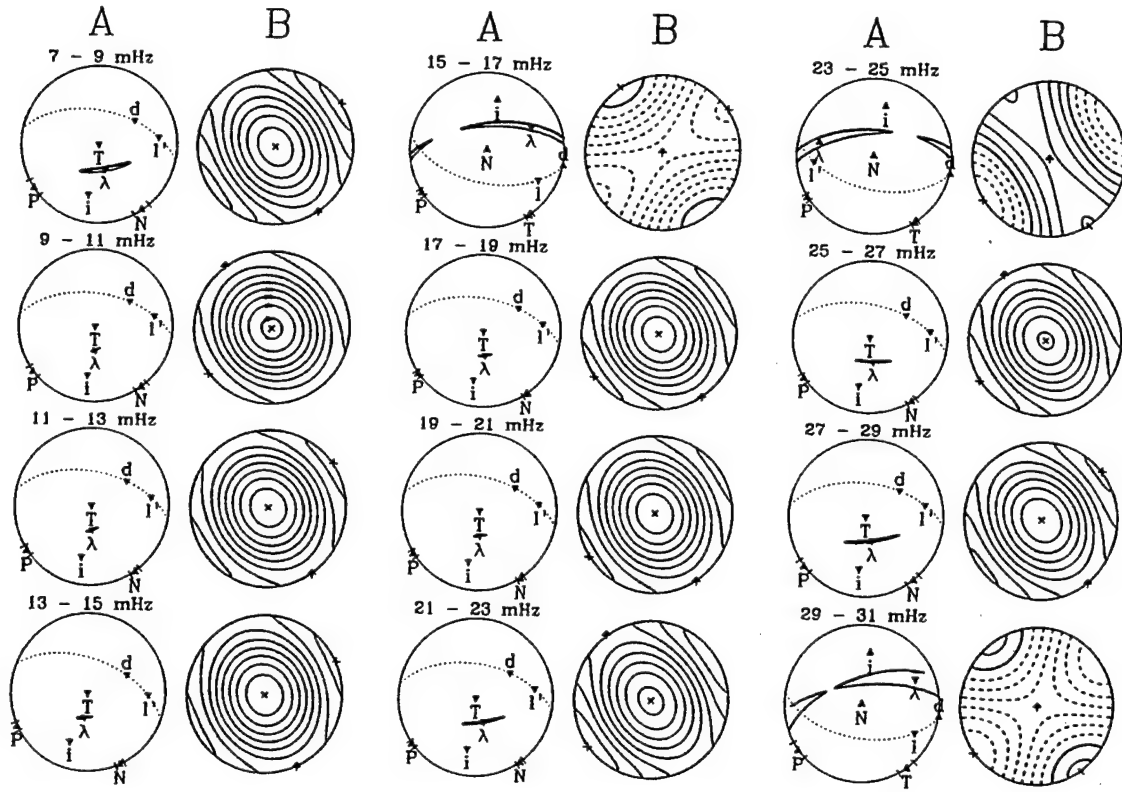


**Figure 12.** Mechanism plots (A) and  $P$ -wave radiation patterns (B) from the (phase-aligned) vertical-component Rayleigh-wave ( $R_1$ ) inversion for the 92/5/21 nuclear explosion near Lop Nor, China. The inversion attempts to recover  $\mathbf{M}(\omega) = \mathbf{M}_I(\omega) + \mathbf{M}_D(\omega)$ ; however,  $m_{r\theta}$  and  $m_{r\phi}$  are projected out. The resulting moment tensor,  $\mathbf{M}(\omega)$ , is relatively stable across the frequency range and exhibits a significant isotropic component, evident by the deviation of the mechanism vector,  $\hat{\lambda}$  from the great-circle of deviatoric sources. The angular distance between  $\hat{\lambda}$  and  $\hat{i}$  measures the size of the isotropic component.

Figure 14 displays a frequency-averaged moment tensor using both surface-wave and body-wave data. Removing the isotropic component ( $M_I = 3.1 \pm 0.3 \times 10^{17}$  Nm) leads to the deviatoric moment tensor ( $M_D = 1.9 \pm 0.2 \times 10^{17}$  Nm) shown. The mechanism plot reveals an insignificant contribution of a CLVD component; it is virtually indistinguishable from a double-couple. The best-fitting double-couple mechanism is displayed separately to facilitate a comparison with the thrust-fault mechanism obtained from the inversion of the transverse-component data. These two independently derived mechanisms (and the scalar moments) are quite similar (Table 1), reassuring us that the inversion of the vertical-component data successfully separated isotropic and deviatoric components. The tectonic release component determined from our inversions is also consistent with the limited amount of geologic information available for this area [Matzko, 1994]. Gao and Richards [1994], investigating earthquakes near the Lop Nor nuclear test site, find a predominance of reverse-faulting events striking NW to SE, in good agreement with our results.

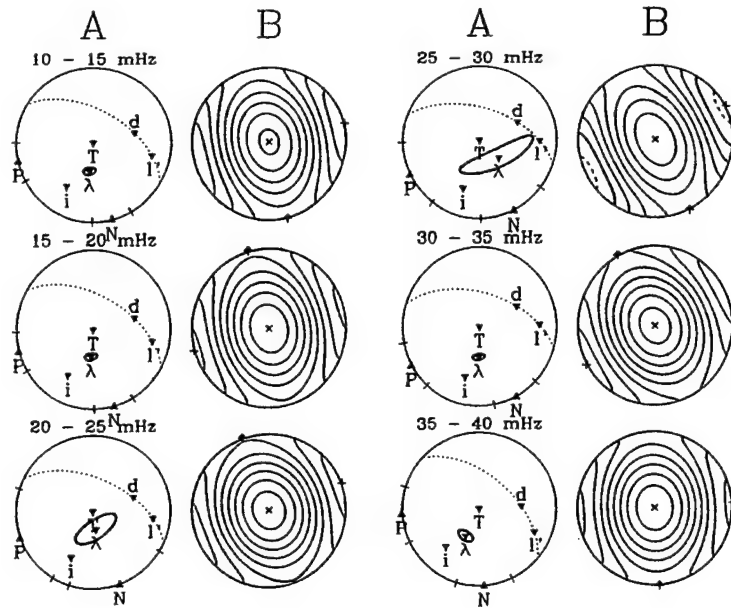


**Figure 13.** Mechanism plots (A) and *P*-wave radiation patterns (B) from the (phase-aligned) moment-tensor inversion using the body-wave portion of vertical-component records that arrive prior to  $R_1$  for the 92/5/21 nuclear test near Lop Nor, China. The resulting moment tensor,  $M(\omega)$  ( $m_{r\theta}$  and  $m_{r\phi}$  are projected out) agrees well with the predominant mechanism found from the Rayleigh-wave inversion.

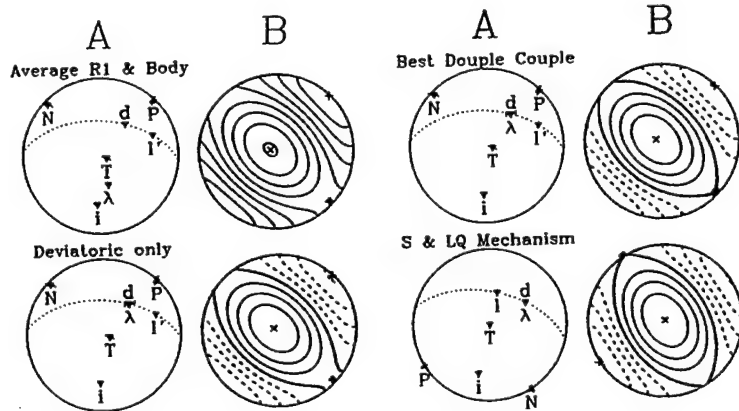


**Figure 14.** Mechanism plots (A) and *P*-wave radiation patterns (B) averaged over frequency bands from the surface-wave and body-wave inversions. The proximity of the mechanism vector  $\hat{\lambda}$  to  $\hat{i}$  on the focal sphere illustrates the strong isotropic component. The deviatoric component of the moment tensor is nearly a double-couple, and differs only slightly from the best fitting pure double-couple mechanism. For comparison, the dip-slip double-couple mechanism obtained from inverting the transverse-component data is also depicted. Double-couple source parameters are listed in Table 1.

**Table 1.** Source parameters of 92/5/21 Lop Nor nuclear test

Data	$M_I$ ( $10^{17}$ Nm)	$M_D$ ( $10^{17}$ Nm)	$M_D/M_I$	$\delta^\dagger$	$\lambda^\dagger$	$\phi_S^\dagger$
$R_1$ and body waves	$3.1 \pm 0.3$	$1.9 \pm 0.2$	$0.61 \pm 0.01$	$48^\circ$	$98^\circ$	$320^\circ$
$G_1$ and $S_H$ waves	0	$1.7 \pm 0.1$		$45^\circ$	$90^\circ$	$329^\circ$

$^\dagger$ Dip,  $\delta$ , slip,  $\lambda$ , and strike,  $\phi_S$ , of best-fitting double-couple mechanism.

## Summary and Conclusions

We have developed a methodology for studying explosion sources that is based on the recovery of the broad-band moment-rate tensor,  $\mathbf{M}(\omega)$ , utilizing both body waves and surface waves. We parameterize the source as being composed of an isotropic and a deviatoric component, i.e.,  $\mathbf{M}(\omega) = \mathbf{M}_I(\omega) + \mathbf{M}_D(\omega)$ . This comprehensive approach encompasses many source parameter diagnostics that have been traditionally used to discriminate nuclear explosions from chemical explosions and earthquakes and has the potential to provide new discrimination tools. Our formalism uses synthetic seismograms to improve the localization of signal measurements in both time and frequency domains. We employ body waves and surface waves from vertical component recordings to invert for  $\mathbf{M}(\omega)$ . Transverse-component  $S_H$  and Love waves provide independent estimates for  $\mathbf{M}_D(\omega)$ , albeit with an intrinsic ambiguity between strike-slip and dip-slip mechanisms.

In our initial year of funding we have accomplished the following tasks:

- (1) We have developed procedures for inverting 3-component seismic data for moment-tensor representations of nuclear explosions. These algorithms have the following features:
  - (a) they allow for the facts that explosion sources are located at very shallow depths by projecting out the  $m_{r\theta}$  and  $m_{r\phi}$  components,
  - (b) they allow for a source mechanism composed of both isotropic and deviatoric components, and
  - (c) they incorporate 3-D propagation models.
- (2) We have validated our moment-tensor inversion algorithms using a synthetic test case with a known moment-tensor source, containing both isotropic and deviatoric components. The source inversions yield stable and self-consistent results across a broad frequency range using both body waves and surface waves (Figures 1–5).
- (3) We have successfully applied graphical display tools, developed for assessing deviatoric earthquakes, to sources with a significant dilatational component. These plots provide an immediate assessment of various features of the mechanism; for example, the relative importance of isotropic and deviatoric (tectonic) contributions to the moment release (Figures 5, 12–14).
- (4) We have successfully applied algorithms to invert source spectra for source time functions. These inversions employ a quadratic programming algorithm that allows various types of time-dependent constraints to be imposed, including smoothness constraints and one-sided constraints.



(5) To improve our understanding of tectonic release in a variety of geologic settings, we have focused on the Chinese nuclear test site near Lop Nor, which has received less attention than the U.S. and Soviet test sites. Using recordings from the 92/5/21 Chinese nuclear test we have obtained moment-tensor solutions for both isotropic and deviatoric mechanisms. The deviatoric component of moment release for this nuclear test is significant ( $M_T/M_I = 0.61 \pm 0.01$ ), and has a negligible non-double-couple component (Figure 14). The best-fitting double-couple shows a reverse-faulting mechanism (Table 1), consistent with focal mechanisms from earthquakes near the Lop Nor nuclear test site. Transverse-component data ( $S_H$  and Love waves), although ambiguous by themselves, provide an independent confirmation for  $M_D$  derived from vertical-component recordings (Figure 14). The network-averaged amplitude spectrum rolls off above 0.04 Hz, indicating a decrease in the size of the tectonic component (Figure 9) with frequency. The source-time function associated with the deviatoric mechanism,  $f_D(t)$ , shows some complexity, with a sharp pulse in moment release followed by a long, smooth tail (Figure 11). Although we must still examine potential sources of bias, we hypothesize that the pulse-like component is caused by scattering of energy from the explosion into  $S_H$ -polarized waves, perhaps by near-source lateral structure, and the smoothly varying component is earthquake-like radiation due to tectonic release.

Tectonic release can lead to biased estimates of  $M_I(\omega)$ . Furthermore, the detection threshold for a given explosion yield also depends on the amount of tectonic energy released by the explosion. It is therefore important to better understand how geology and explosion size/depth, influence the amount of tectonic release – in particular as a function of frequency. Gaining new insights into how tectonic release scales with frequency and explosion yield/depth should also lead to a better understanding on how high-frequency discriminants such as  $P/L_g$  are affected by tectonic release. At present, we are addressing these questions by applying our source recovery algorithms to data from a number of nuclear tests of varying sizes. To better quantify the importance of tectonic release as a function of frequency, we are adapting our source inversion tools to higher frequencies. We are also investigating formulations for directly inverting for the relative contributions of tectonic and isotropic components as a function of frequency. At higher frequencies, apparent attenuation due to scattering as well as the effects of frequency-dependent intrinsic attenuation are expected to dominate the source amplitude spectrum, making an inversion algorithm based on the relative magnitude of tectonic and explosion components desirable.



## References

- Aki, K., and P. Richards, *Quantitative Seismology*, 557 pp., Freeman and Co., San Francisco, 1980.
- Aki, K., and Y.-B. Tsai, Mechanism of Love-wave excitation by explosive sources, *J. Geophys. Res.*, 77, 1452-1475, 1972.
- Archambeau, C. B., The theory of stress wave radiation from explosions in prestressed media, *Geophys. J. R. Astron. Soc.*, 29, 329-366, 1972.
- Backus, G., Seismic sources with observable glut moments of total degree two or less, *Geophys. J. R. Astron. Soc.*, 51, 1-25, 1977.
- Brune, J. N., and P. W. Pomeroy, Surface wave radiation patterns for underground nuclear explosions and small-magnitude earthquakes, *J. Geophys. Res.*, 68, 5005-5028, 1963.
- Denny, M. D., and L. R. Johnson, The explosion seismic source function: models and scaling laws reviewed, in *Explosion source phenomenology*, edited by S. Taylor, H. Patton, and P. Richards, *Geophysical Monograph Series*, 65, pp. 1-24, AGU, Washington, D.C., 1991.
- Dziewonski, A. M., and D. L. Anderson, Preliminary reference Earth model, *Phys. Earth Planet. Inter.*, 25, 297-356, 1981.
- Ekström, G., and P. G. Richards, Empirical measurements of tectonic moment release in nuclear explosions from teleseismic surface waves and body waves, *Geophys. J. Int.*, 117, 120-140, 1994.
- Gaherty, J. B., and T. H. Jordan, Lehmann Discontinuity as the base of an anisotropic layer beneath continents, *Science*, 268, 1468-1471, 1995.
- Gao, L., and P. G. Richards, Studies of earthquakes on and near the Lop Nor, China, nuclear test site, *Proceedings of the 16th Annual Seismic Research Symposium*, 106-112, 1994, PL-TR-94-2217, ADA284667
- Gee, L. S., and T. H. Jordan, Generalized seismological data functionals, *Geophys. J. Int.*, 111, 363-390, 1992.
- Given, J. W., and G. R. Mellman, Estimating explosion and tectonic release source parameters of underground nuclear explosions from Rayleigh and Love wave observations, *US Air Force Geophysics Laboratory, MA, Final Report-Part 1, AFGL-TR-86-0171(I)*, 1986, AFGL-TR-86-0171(I), ADB110040 (approved for public release on 25 March 1992).
- Helle, H. B., and E. Rygg, Determination of tectonic release from surface waves generated by nuclear explosions in Eastern Kazakhstan, *Bull. Seismol. Soc. Am.*, 74, 1883-1898, 1984.
- Ihmlé, P. F., P. Harabaglia, and T. H. Jordan, Teleseismic detection of a slow precursor to the great 1989 Macquarie Ridge earthquake, *Science*, 261, 177-183, 1993.
- Ihmlé, P. F., and T. H. Jordan, Teleseismic search for slow precursors to large earthquakes, *Science*, 266, 1547-1551, 1994.
- Ihmlé, P. F., and T. H. Jordan, Source time function of the great 1994 Bolivia deep earthquake by waveform and spectral inversions, *Geophys. Res. Lett.*, 22, 2253-2256, 1995.
- Kanamori, H., and J. W. Given, Use of long-period surface waves for rapid determination of earthquake-source parameters, *Phys. Earth Planet. Inter.*, 27, 8-31, 1981.

- Matzko, J. R., Geology of the Chinese nuclear test site near Lop Nor, Xinjiang Uygur autonomous region, China, *Eng. Geol.*, 36, 173-181, 1994.
- Patton, H. J., Surface-wave generation by underground nuclear explosions releasing tectonic strain, *Lawrence Livermore National Laboratory, Livermore, CA, UCRL-53062*, 16, 1980.
- Patton, H. J., Source models of the Harzer explosion from regional observations of fundamental-mode and higher mode surface waves, *Bull. Seismol. Soc. Am.*, 78, 1133-1157, 1988.
- Patton, H. J., Seismic moment estimation and the scaling of the long-period explosion source spectrum, in *Explosion source phenomenology*, edited by S. Taylor, H. Patton, and P. Richards, *Geophysical Monograph Series*, 65, pp. 171-183, AGU, Washington, D.C., 1991.
- Press, F., and C. Archambeau, Release of tectonic strain by underground nuclear explosions, *J. Geophys. Res.*, 67, 337-343, 1962.
- Riedesel, M. A., and T. H. Jordan, Display and assessment of seismic moment tensors, *Bull. Seismol. Soc. Am.*, 79, 85-100, 1989.
- Silver, P. G., and T. H. Jordan, Optimal estimation of scalar seismic moment, *Geophys. J. R. Astron. Soc.*, 70, 755-787, 1982.
- Su, W.-J., R. L. Woodward, and A. M. Dziewonski, Degree 12 model of shear velocity heterogeneity in the mantle, *J. Geophys. Res.*, 99, 6945-6980, 1994.
- Toksöz, M. N., A. Ben-Menahem, and D. G. Harkrider, Determination of source parameters of explosions and earthquakes by amplitude equalization of seismic surface waves, 1. Underground nuclear explosions, *J. Geophys. Res.*, 69, 4355-4366, 1964.
- Wallace, T. C., Body wave observations of tectonic release, in *Explosion source phenomenology*, edited by S. Taylor, H. Patton, and P. Richards, *Geophysical Monograph Series*, 65, pp. 161-170, AGU, Washington, D.C., 1991.
- Wallace, T. C., D. V. Helmberger, and G. R. Engen, Evidence of tectonic release from underground nuclear explosions in long-period P waves, *Bull. Seismol. Soc. Am.*, 73, 593-613, 1983.
- Wallace, T. C., D. V. Helmberger, and G. R. Engen, Evidence of tectonic release from underground nuclear explosions in long-period S waves, *Bull. Seismol. Soc. Am.*, 75, 157-174, 1985.
- Walter, W. R., and H. J. Patton, Tectonic release from the soviet joint verification experiment, *Geophys. Res. Lett.*, 17, 1517-1520, 1990.
- Woodhouse, J. H., and A. M. Dziewonski, Mapping the upper mantle: three-dimensional modeling of earth structure by inversion of seismic waveforms, *J. Geophys. Res.*, 89, 5953-5986, 1984.
- Zhang, J., Source characterization using simplified waveforms: tests on earthquakes and nuclear explosions in Xinjiang, China, *Proceedings of the 18th annual seismic research symposium on monitoring a comprehensive test ban treaty*, 429-438, 1996. PL-TR-96-2153, ADA313692.

THOMAS AHRENS  
SEISMOLOGICAL LABORATORY 252-21  
CALIFORNIA INSTITUTE OF TECHNOLOGY  
PASADENA, CA 91125

RALPH ALEWINE  
NTPO  
1901 N. MOORE STREET, SUITE 609  
ARLINGTON, VA 22209

SHELTON ALEXANDER  
PENNSYLVANIA STATE UNIVERSITY  
DEPARTMENT OF GEOSCIENCES  
537 DEIKE BUILDING  
UNIVERSITY PARK, PA 16801

MUAWIA BARAZANGI  
INSTITUTE FOR THE STUDY OF THE CONTINENTS  
3126 SNEE HALL  
CORNELL UNIVERSITY  
ITHACA, NY 14853

RICHARD BARDZELL  
ACIS  
DCI/ACIS  
WASHINGTON, DC 20505

T.G. BARKER  
MAXWELL TECHNOLOGIES  
P.O. BOX 23558  
SAN DIEGO, CA 92123

DOUGLAS BAUMGARDT  
ENSCO INC.  
5400 PORT ROYAL ROAD  
SPRINGFIELD, VA 22151

THERON J. BENNETT  
MAXWELL TECHNOLOGIES  
11800 SUNRISE VALLEY DRIVE SUITE 1212  
RESTON, VA 22091

WILLIAM BENSON  
NAS/COS  
ROOM HA372  
2001 WISCONSIN AVE. NW  
WASHINGTON, DC 20007

JONATHAN BERGER  
UNIVERSITY OF CA, SAN DIEGO  
SCRIPPS INSTITUTION OF OCEANOGRAPHY IGPP, 0225  
9500 GILMAN DRIVE  
LA JOLLA, CA 92093-0225

ROBERT BLANDFORD  
AFTAC  
1300 N. 17TH STREET  
SUITE 1450  
ARLINGTON, VA 22209-2308

STEVEN BRATT  
NTPO  
1901 N. MOORE STREET, SUITE 609  
ARLINGTON, VA 22209

RHETT BUTLER  
IRIS  
1616 N. FORT MEYER DRIVE  
SUITE 1050  
ARLINGTON, VA 22209

LESLIE A. CASEY  
DOE  
1000 INDEPENDENCE AVE. SW  
NN-40  
WASHINGTON, DC 20585-0420

CATHERINE DE GROOT-HEDLIN  
SCRIPPS INSTITUTION OF OCEANOGRAPHY  
UNIVERSITY OF CALIFORNIA, SAN DIEGO  
INSTITUTE OF GEOPHYSICS AND PLANETARY PHYSICS  
LA JOLLA, CA 92093

STANLEY DICKINSON  
AFOSR  
110 DUNCAN AVENUE, SUITE B115  
BOLLING AFB  
WASHINGTON, D.C. 20332-001

SEAN DORAN  
ACIS  
DCI/ACIS  
WASHINGTON, DC 20505

DIANE I. DOSER  
DEPARTMENT OF GEOLOGICAL SCIENCES  
THE UNIVERSITY OF TEXAS AT EL PASO  
EL PASO, TX 79968

RICHARD J. FANTEL  
BUREAU OF MINES  
DEPT OF INTERIOR, BLDG 20  
DENVER FEDERAL CENTER  
DENVER, CO 80225

JOHN FILSON  
ACIS/TMG/NTT  
ROOM 6T11 NHB  
WASHINGTON, DC 20505

MARK D. FISK  
MISSION RESEARCH CORPORATION  
735 STATE STREET  
P.O. DRAWER 719  
SANTA BARBARA, CA 93102-0719

LORI GRANT  
MULTIMAX, INC.  
311C FOREST AVE. SUITE 3  
PACIFIC GROVE, CA 93950

I. N. GUPTA  
MULTIMAX, INC.  
1441 MCCORMICK DRIVE  
LARGO, MD 20774

JAMES HAYES  
NSF  
4201 WILSON BLVD., ROOM 785  
ARLINGTON, VA 22230

MICHAEL HEDLIN  
UNIVERSITY OF CALIFORNIA, SAN DIEGO  
SCRIPPS INSTITUTION OF OCEANOGRAPHY IGPP, 0225  
9500 GILMAN DRIVE  
LA JOLLA, CA 92093-0225

EUGENE HERRIN  
SOUTHERN METHODIST UNIVERSITY  
DEPARTMENT OF GEOLOGICAL SCIENCES  
DALLAS, TX 75275-0395

VINDELL HSU  
HQ/AFTAC/TTR  
1030 S. HIGHWAY A1A  
PATRICK AFB, FL 32925-3002

RONG-SONG JIH  
PHILLIPS LABORATORY  
EARTH SCIENCES DIVISION  
29 RANDOLPH ROAD  
HANSCOM AFB, MA 01731-3010

LAWRENCE LIVERMORE NATIONAL LABORATORY  
ATTN: TECHNICAL STAFF (PLS ROUTE)  
PO BOX 808, MS L-200  
LIVERMORE, CA 94551

LAWRENCE LIVERMORE NATIONAL LABORATORY  
ATTN: TECHNICAL STAFF (PLS ROUTE)  
PO BOX 808, MS L-221  
LIVERMORE, CA 94551

ROBERT GEIL  
DOE  
PALAIS DES NATIONS, RM D615  
GENEVA 10, SWITZERLAND

HENRY GRAY  
SMU STATISTICS DEPARTMENT  
P.O. BOX 750302  
DALLAS, TX 75275-0302

DAVID HARKRIDER  
PHILLIPS LABORATORY  
EARTH SCIENCES DIVISION  
29 RANDOLPH ROAD  
HANSCOM AFB, MA 01731-3010

THOMAS HEARN  
NEW MEXICO STATE UNIVERSITY  
DEPARTMENT OF PHYSICS  
LAS CRUCES, NM 88003

DONALD HELMBERGER  
CALIFORNIA INSTITUTE OF TECHNOLOGY  
DIVISION OF GEOLOGICAL & PLANETARY SCIENCES  
SEISMOLOGICAL LABORATORY  
PASADENA, CA 91125

ROBERT HERRMANN  
ST. LOUIS UNIVERSITY  
DEPARTMENT OF EARTH & ATMOSPHERIC SCIENCES  
3507 LACLEDE AVENUE  
ST. LOUIS, MO 63103

ANTHONY IANNACCHIONE  
BUREAU OF MINES  
COCHRANE MILL ROAD  
PO BOX 18070  
PITTSBURGH, PA 15236-9986

THOMAS JORDAN  
MASSACHUSETTS INSTITUTE OF TECHNOLOGY  
EARTH, ATMOSPHERIC & PLANETARY SCIENCES  
77 MASSACHUSETTS AVENUE, 54-918  
CAMBRIDGE, MA 02139

LAWRENCE LIVERMORE NATIONAL LABORATORY  
ATTN: TECHNICAL STAFF (PLS ROUTE)  
PO BOX 808, MS L-207  
LIVERMORE, CA 94551

LAWRENCE LIVERMORE NATIONAL LABORATORY  
ATTN: TECHNICAL STAFF (PLS ROUTE)  
LLNL  
PO BOX 808, MS L-175  
LIVERMORE, CA 94551

LAWRENCE LIVERMORE NATIONAL LABORATORY  
ATTN: TECHNICAL STAFF (PLS ROUTE)  
PO BOX 808, MS L-208  
LIVERMORE, CA 94551

LAWRENCE LIVERMORE NATIONAL LABORATORY  
ATTN: TECHNICAL STAFF (PLS ROUTE)  
PO BOX 808, MS L-202  
LIVERMORE, CA 94551

LAWRENCE LIVERMORE NATIONAL LABORATORY  
ATTN: TECHNICAL STAFF (PLS ROUTE)  
PO BOX 808, MS L-195  
LIVERMORE, CA 94551

LAWRENCE LIVERMORE NATIONAL LABORATORY  
ATTN: TECHNICAL STAFF (PLS ROUTE)  
PO BOX 808, MS L-205  
LIVERMORE, CA 94551

THORNE LAY  
UNIVERSITY OF CALIFORNIA, SANTA CRUZ  
EARTH SCIENCES DEPARTMENT  
EARTH & MARINE SCIENCE BUILDING  
SANTA CRUZ, CA 95064

ANATOLI L. LEVSHIN  
DEPARTMENT OF PHYSICS  
UNIVERSITY OF COLORADO  
CAMPUS BOX 390  
BOULDER, CO 80309-0309

DONALD A. LINGER  
DNA  
6801 TELEGRAPH ROAD  
ALEXANDRIA, VA 22310

LOS ALAMOS NATIONAL LABORATORY  
ATTN: TECHNICAL STAFF (PLS ROUTE)  
PO BOX 1663, MS F659  
LOS ALAMOS, NM 87545

LOS ALAMOS NATIONAL LABORATORY  
ATTN: TECHNICAL STAFF (PLS ROUTE)  
PO BOX 1663, MS F665  
LOS ALAMOS, NM 87545

LOS ALAMOS NATIONAL LABORATORY  
ATTN: TECHNICAL STAFF (PLS ROUTE)  
PO BOX 1663, MS D460  
LOS ALAMOS, NM 87545

LOS ALAMOS NATIONAL LABORATORY  
ATTN: TECHNICAL STAFF (PLS ROUTE)  
PO BOX 1663, MS C335  
LOS ALAMOS, NM 87545

GARY MCCARTOR  
SOUTHERN METHODIST UNIVERSITY  
DEPARTMENT OF PHYSICS  
DALLAS, TX 75275-0395

KEITH MCLAUGHLIN  
MAXWELL TECHNOLOGIES  
P.O. BOX 23558  
SAN DIEGO, CA 92123

BRIAN MITCHELL  
DEPARTMENT OF EARTH & ATMOSPHERIC SCIENCES  
ST. LOUIS UNIVERSITY  
3507 LACLEDE AVENUE  
ST. LOUIS, MO 63103

RICHARD MORROW  
USACDA/VI  
320 21ST STREET, N.W.  
WASHINGTON, DC 20451

JOHN MURPHY  
MAXWELL TECHNOLOGIES  
11800 SUNRISE VALLEY DRIVE SUITE 1212  
RESTON, VA 22091

JAMES NI  
NEW MEXICO STATE UNIVERSITY  
DEPARTMENT OF PHYSICS  
LAS CRUCES, NM 88003

JOHN ORCUTT  
INSTITUTE OF GEOPHYSICS AND PLANETARY PHYSICS  
UNIVERSITY OF CALIFORNIA, SAN DIEGO  
LA JOLLA, CA 92093

PACIFIC NORTHWEST NATIONAL LABORATORY  
ATTN: TECHNICAL STAFF (PLS ROUTE)  
PO BOX 999, MS K6-48  
RICHLAND, WA 99352

PACIFIC NORTHWEST NATIONAL LABORATORY  
ATTN: TECHNICAL STAFF (PLS ROUTE)  
PO BOX 999, MS K7-34  
RICHLAND, WA 99352

PACIFIC NORTHWEST NATIONAL LABORATORY  
ATTN: TECHNICAL STAFF (PLS ROUTE)  
PO BOX 999, MS K6-40  
RICHLAND, WA 99352

PACIFIC NORTHWEST NATIONAL LABORATORY  
ATTN: TECHNICAL STAFF (PLS ROUTE)  
PO BOX 999, MS K5-12  
RICHLAND, WA 99352

PACIFIC NORTHWEST NATIONAL LABORATORY  
ATTN: TECHNICAL STAFF (PLS ROUTE)  
PO BOX 999, MS K5-12  
RICHLAND, WA 99352

KEITH PRIESTLEY  
DEPARTMENT OF EARTH SCIENCES  
UNIVERSITY OF CAMBRIDGE  
MADINGLEY RISE, MADINGLEY ROAD  
CAMBRIDGE, CB3 0EZ UK

PAUL RICHARDS  
COLUMBIA UNIVERSITY  
LAMONT-DOHERTY EARTH OBSERVATORY  
PALISADES, NY 10964

CHANDAN SAIKIA  
WOODWARD-CLYDE FEDERAL SERVICES  
566 EL DORADO ST., SUITE 100  
PASADENA, CA 91101-2560

SANDIA NATIONAL LABORATORY  
ATTN: TECHNICAL STAFF (PLS ROUTE)  
DEPT. 5791  
MS 0567, PO BOX 5800  
ALBUQUERQUE, NM 87185-0567

SANDIA NATIONAL LABORATORY  
ATTN: TECHNICAL STAFF (PLS ROUTE)  
DEPT. 5704  
MS 0655, PO BOX 5800  
ALBUQUERQUE, NM 87185-0655

THOMAS SERENO JR.  
SCIENCE APPLICATIONS INTERNATIONAL  
CORPORATION  
10260 CAMPUS POINT DRIVE  
SAN DIEGO, CA 92121

ROBERT SHUMWAY  
410 MRAK HALL  
DIVISION OF STATISTICS  
UNIVERSITY OF CALIFORNIA  
DAVIS, CA 95616-8671

PACIFIC NORTHWEST NATIONAL LABORATORY  
ATTN: TECHNICAL STAFF (PLS ROUTE)  
PO BOX 999, MS K7-22  
RICHLAND, WA 99352

PACIFIC NORTHWEST NATIONAL LABORATORY  
ATTN: TECHNICAL STAFF (PLS ROUTE)  
PO BOX 999, MS K6-84  
RICHLAND, WA 99352

FRANK PILOTTE  
HQ/AFTAC/TT  
1030 S. HIGHWAY A1A  
PATRICK AFB, FL 32925-3002

JAY PULLI  
RADIX SYSTEMS, INC.  
6 TAFT COURT  
ROCKVILLE, MD 20850

DAVID RUSSELL  
HQ AFTAC/TTR  
1030 SOUTH HIGHWAY A1A  
PATRICK AFB, FL 32925-3002

SANDIA NATIONAL LABORATORY  
ATTN: TECHNICAL STAFF (PLS ROUTE)  
DEPT. 5704  
MS 0979, PO BOX 5800  
ALBUQUERQUE, NM 87185-0979

SANDIA NATIONAL LABORATORY  
ATTN: TECHNICAL STAFF (PLS ROUTE)  
DEPT. 9311  
MS 1159, PO BOX 5800  
ALBUQUERQUE, NM 87185-1159

SANDIA NATIONAL LABORATORY  
ATTN: TECHNICAL STAFF (PLS ROUTE)  
DEPT. 5736  
MS 0655, PO BOX 5800  
ALBUQUERQUE, NM 87185-0655

AVI SHAPIRA  
SEISMOLOGY DIVISION  
THE INSTITUTE FOR PETROLEUM RESEARCH AND  
GEOPHYSICS  
P.O.B. 2286, NOLON 58122 ISRAEL

MATTHEW SIBOL  
ENSCO, INC.  
445 PINEDA COURT  
MELBOURNE, FL 32940

DAVID SIMPSON  
IRIS  
1616 N. FORT MEYER DRIVE  
SUITE 1050  
ARLINGTON, VA 22209

BRIAN SULLIVAN  
BOSTON COLLEGE  
INSTITUTE FOR SPACE RESEARCH  
140 COMMONWEALTH AVENUE  
CHESTNUT HILL, MA 02167

NAFI TOKSOZ  
EARTH RESOURCES LABORATORY, M.I.T.  
42 CARLTON STREET, E34-440  
CAMBRIDGE, MA 02142

GREG VAN DER VINK  
IRIS  
1616 N. FORT MEYER DRIVE  
SUITE 1050  
ARLINGTON, VA 22209

TERRY WALLACE  
UNIVERSITY OF ARIZONA  
DEPARTMENT OF GEOSCIENCES  
BUILDING #77  
TUCSON, AZ 85721

JAMES WHITCOMB  
NSF  
NSF/ISC OPERATIONS/EAR-785  
4201 WILSON BLVD., ROOM 785  
ARLINGTON, VA 22230

JIANG XIE  
COLUMBIA UNIVERSITY  
LAMONT DOHERTY EARTH OBSERVATORY  
ROUTE 9W  
PALISADES, NY 10964

OFFICE OF THE SECRETARY OF DEFENSE  
DDR&E  
WASHINGTON, DC 20330

TACTEC  
BATTELLE MEMORIAL INSTITUTE  
505 KING AVENUE  
COLUMBUS, OH 43201 (FINAL REPORT)

PHILLIPS LABORATORY  
ATTN: GPE  
29 RANDOLPH ROAD  
HANSCOM AFB, MA 01731-3010

JEFFRY STEVENS  
MAXWELL TECHNOLOGIES  
P.O. BOX 23558  
SAN DIEGO, CA 92123

DAVID THOMAS  
ISEE  
29100 AURORA ROAD  
CLEVELAND, OH 44139

LAWRENCE TURNBULL  
ACIS  
DCI/ACIS  
WASHINGTON, DC 20505

FRANK VERNON  
UNIVERSITY OF CALIFORNIA, SAN DIEGO  
SCRIPPS INSTITUTION OF OCEANOGRAPHY IGPP, 0225  
9500 GILMAN DRIVE  
LA JOLLA, CA 92093-0225

DANIEL WEILL  
NSF  
EAR-785  
4201 WILSON BLVD., ROOM 785  
ARLINGTON, VA 22230

RU SHAN WU  
UNIVERSITY OF CALIFORNIA SANTA CRUZ  
EARTH SCIENCES DEPT.  
1156 HIGH STREET  
SANTA CRUZ, CA 95064

JAMES E. ZOLLWEG  
BOISE STATE UNIVERSITY  
GEOSCIENCES DEPT.  
1910 UNIVERSITY DRIVE  
BOISE, ID 83725

DEFENSE TECHNICAL INFORMATION CENTER  
8725 JOHN J. KINGMAN ROAD  
FT BELVOIR, VA 22060-6218 (2 COPIES)

PHILLIPS LABORATORY  
ATTN: XPG  
29 RANDOLPH ROAD  
HANSCOM AFB, MA 01731-3010

PHILLIPS LABORATORY  
ATTN: TSML  
5 WRIGHT STREET  
HANSCOM AFB, MA 01731-3004

PHILLIPS LABORATORY  
ATTN: PL/SUL  
3550 ABERDEEN AVE SE  
KIRTLAND, NM 87117-5776 (2 COPIES)